Asymmetric Coordination of Single-atom Co Sites Boosts Dehydrogenation Catalysis of HCOOH

Hu Liu, Qian Lei, Ruoyan Miao, Mingzi Sun, Chuanjian Qin, Liang Zhang, Gan Ye, Yao Yao*, Bolong Huang*, Zhenhui Ma**

H. Liu, Q. Lei, R. Miao, C. Qin, G. Ye, L. Zhang, Prof. Y. Yao
School of Chemistry and Chemical Engineering and School of Civil Engineering, Xi'an University of Architecture and Technology, Xi'an 710055, China.
E-mail: liuhu@xauat.edu.cn, yaoy@xauat.edu.cn

M. Sun, Prof. B. Huang
Department of Applied Biology and Chemical Technology, The Hong Kong Polytechnic University, Hung Hom, Kowloon, Hong Kong SAR, China.
E-mail: bhuang@polyu.edu.hk

Prof. Z. Ma
Department of Physics, Beijing Technology and Business University, 100048, Beijing, China.

Keywords: atomic Co, single-atom site, asymmetric coordination, nitrogen-doped carbon nanowires network, formic acid dehydrogenation, clean energy

Abstract: Tuning asymmetric coordination of metal single-atom (SA) sites can provide a new opportunity for optimizing the electronic structure of catalysts to achieve highly efficient catalysis, however, achieving such controllable design remains a grand challenge. Herein, we report asymmetrically coordinated Co-N_4P SA sites as a new catalyst system for achieving superior dehydrogenation catalysis of formic acid (HCOOH). X-ray absorption fine structure results show that the Co atom is coordinated by four N atoms and one asymmetric P atom, forming the unique Co-N_4P SA sites. The asymmetrically coordinated Co-N_4P SA sites exhibit a dehydrogenation activity of 2185.5 h^{-1} with 100% selectivity and outstanding stability for HCOOH under mild conditions, which is 5-fold higher than that of symmetrically coordinated Co-N_4 SA sites. Theoretical calculations further reveal that the asymmetric P sites not only boost the C-H bond cleavage of HCOO* by largely reducing the energy barrier but also facilitate the proton adsorptions to achieve the fast generation of H_2 in Co-N_4P SA sites, which is the key reason for achieving efficient dehydrogenation of HCOOH. This work opens a new way for rationally designing novel SA sites to achieve efficient catalysis.

Introduction

The increasing energy demand drives researchers to search for renewable energy for building an energy-sustainable society [1-3]. Hydrogen (H_2), as a clean energy, has attracted great attention because of its high energy density, zero pollution and zero-carbon emission [4-7]. Among various H_2 production methods [8-13], the dehydrogenation of formic acid (HCOOH) is a promising and sustainable approach due to its high volumetric (53 $g \cdot L^{-1}$) and gravimetric (4.4 *wt*%) H_2 storage capacities, high energy density (1.77 $kW \cdot h \cdot L^{-1}$), favorable thermodynamics characteristics, nontoxicity and liquid state at room temperature [14-16]. Especially, HCOOH is a renewable organic molecule, which can be synthesized from the sustainable routes of CO_2 hydrogenation or biomass partial oxidation [17-21]. The key for dehydrogenation catalysis is the development of high-performance catalysts with high activity, high selectivity and outstanding stability.

Noble metal-based nanocatalysts have exhibited certain activity and selectivity towards HCOOH dehydrogenation [22-27], however, they experience the drawbacks of their scarce and high cost. In light of this, exploring non-noble metal single atom (SA) sites with the maximum utilization efficiency and excellent catalytic performance provides a promising opportunity for dehydrogenation catalysis of HCOOH [28-40]. However, the well-known non-noble metal SA sites with symmetrical coordination environments usually show limited catalytic activity and selectivity for HCOOH dehydrogenation [41-44].

Herein, we report a new strategy to introduce asymmetric P atoms into symmetrically coordinated Co-N_4 SA sites on nitrogen-doped carbon nanowires network, forming unique asymmetrically coordinated Co-N_4P SA sites, for greatly boosting for dehydrogenation catalysis of HCOOH under a mild condition. As-synthesized asymmetrically coordinated Co-N_4P SA sites display 5-fold higher activity than that of symmetrically coordinated Co-N_4 SA sites, along with high selectivity of 100% and superb stability towards HCOOH dehydrogenation under mild conditions. DFT calculations reveal the electronic perturbation induced by the asymmetric coordination environment in Co-N_4P SA sites promotes the C-H bond cleavage of HCOO* by reducing the energy barrier but also accelerates the fast generation of H_2 through improved proton adsorptions in Co-N_4P SA sites.

Results and discussion

The Co-N_4P SA sites supported on nitrogen-doped carbon nanowires network were synthesized by combining wet-chemical and pyrolysis strategies (Supporting Information for details) (**Figure S1**). Both scanning electron microscopy (SEM) and transmission electron microscopy (TEM) images of Co-N_4P SA sites show that the support of Co-N_4P SA sites has nanowire network-like morphology (**Figure S2 & 1a**). We find that the formation of nanowires network-like morphology is only dependent on the feeding amounts of $Co(NO_3)_2{\cdot}6H_2O$ (**Figure S3 & S4**), and asymmetric coordination of SA Co sites can be achieved by tuning the pyrolysis way and feeding amounts of triphenylphosphine (PPh_3) and $Co(NO_3)_2{\cdot}6H_2O$ (**Figure S5 & S6**). The high-angle annular dark-field scanning TEM (HAADF-STEM) image of Co-N_4P SA sites shows that there are countless bright spots, representing Co atoms (**Figure 1b**). The corresponding energy dispersive spectroscopy-STEM (STEM-EDS) mapping results demonstrate that C, N, Co and P elements of Co-N_4P SA sites are uniformly dispersed across the nitrogen-doped carbon nanowires network (**Figure 1c & S7**).

As a control, the Co-N_4 SA sites supported on nitrogen-doped carbon nanowires network with different loading amounts were further synthesized by the similar synthetic method except for the absence of PPh_3 (Supporting Information for details). The Co species from the Co-N_4 SA sites, as well as Co-N_4P SA sites, are also atomically dispersed onto the nitrogen-doped carbon nanowires network (**Figure S8 & S9**). The Co contents of as-synthesized Co-N_4 SA sites and Co-N_4P SA sites on nitrogen-doped carbon nanowires network were determined by inductively coupled plasma-atomic emission spectroscopy (ICP-AES). According to the ICP-AES results, as-synthesized various Co-N_4 SA sites and Co-N_4P SA sites were denoted as 2.8 *wt*% Co-N_4 SA sites, 4.1 *wt*% Co-N_4 SA sites, 5.5 *wt*% Co-N_4 SA sites and 5.3 *wt*% Co-N_4P SA sites, respectively (**Table S1**). The contents of N and P in 5.3 *wt*% Co-N_4P SA sites were evaluated to be nearly 11.4 % and 2.8 % respectively, determined by the EDS and X-ray photoelectron spectroscopy (XPS) spectra, confirming that the stoichiometric ratio of N: P in 5.3 *wt*% Co-N_4P SA sites is 9: 1 (**Figure S10 & Table S2**).

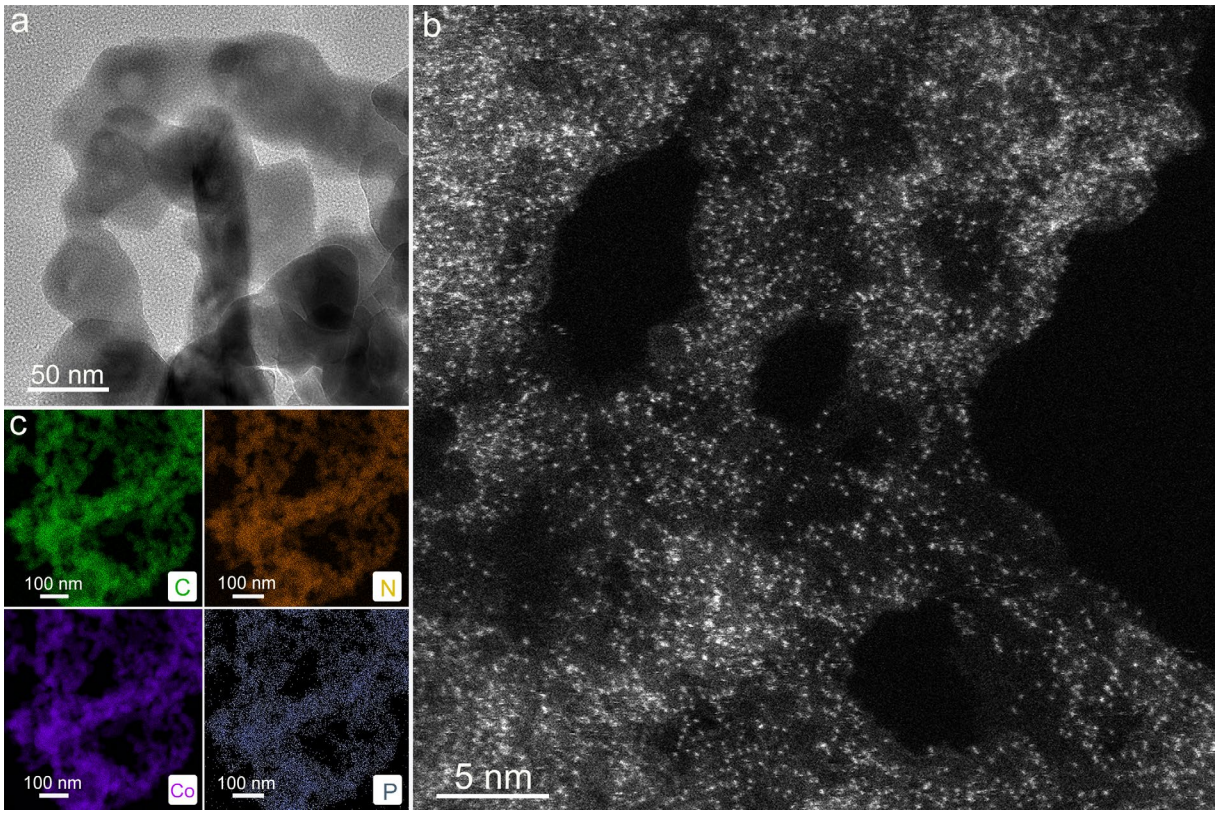

Figure 1. **Microscopic characterization of 5.3 *wt*% SA Co-N$_4$P sites**. (a) TEM image, (b) HAADF-STEM image and (c) elemental maps of 5.3 *wt*% Co-N$_4$P SA sites.

To analyze the atomic structure of 5.3 *wt*% Co-N$_4$P SA sites, the soft X-ray absorption near edge structure (XANES), Raman, powder X-ray diffraction (PXRD) and XPS spectra were carried out. The C K-edge spectrum of 5.3 *wt*% Co-N$_4$P SA sites contains four peaks located at 279.8, 280.9, 284.6 and 300.4 eV, attributed to the antibonding orbitals of π*(C-N), π*(C=C), π*(C-P) and σ*(C-C), respectively (**Figure S11**) [49,50]. Noted that the peak located at 279.8 eV suggests the existence of the C-N-Co bonds in the chemical environment of 5.3 *wt*% Co-N$_4$P SA sites. Two characteristic peaks can be observed at 1604.1 and 1387.8 cm^{-1} in Raman spectra of both 5.5 *wt*% Co-N$_4$ SA sites and 5.3 *wt*% Co-N$_4$P SA sites, corresponding to the G-peak and D-peak of the nitrogen-doped carbon nanowires network, respectively (**Figure 2a**). The C-N, C-P and C=C bonds of 5.3 *wt*% Co-N$_4$P SA sites can be further verified by high-resolution C 1s XPS spectrum (**Figure S12a**). The P-C and P-N bonds were monitored by high-resolution P 2p XPS spectrum (**Figure S12b**). Theoretical P 2p XPS spectrum of 5.3 *wt*% Co-N$_4$P SA sites is consistent with the experimental result (**Figure S12b**). The high-resolution N 1s XPS spectrum in 5.3 *wt*% Co-N$_4$P SA sites was fitted into three peaks, involving a pyridinic N peak at 398.8 eV,

a graphitic N peak at 399.8 eV and a pyrrolic N peak at 401.1 eV (**Figure 2b**) [47,48].

Hard XANES and the extended X-ray absorption fine structure (EXAFS) at Co K-edge were carried out to reveal the detailed structure information of 5.3 *wt*% Co-N_4P SA sites. The Co K-edge absorption edge of 5.3 *wt*% Co-N_4P SA sites locates between those of cobalt phthalocyanine (CoPc) and CoP in the black dotted box of **Figure 2c**, suggesting that Co atoms in 5.3 *wt*% Co-N_4P SA sites possess fewer positive charges than that of CoPc, and more positive charges than that of CoP (**Table S3**). Theoretical C K-edge and Co K-edge XANES spectra are well matched with the experimental results (**Figure S11 & S13**), further confirming the atomic structure of 5.3 *wt*% Co-N_4P SA sites. Note that the coordination environment difference between 5.5 *wt*% Co-N_4 SA sites and 5.3 *wt*% SA Co-N_4P sites can be attributed to the existence of Co-N-P bond in 5.3 *wt*% Co-N_4P SA sites, leading to strong electronic transfer between Co, P and N [45,46]. The Fourier transform (FT) EXAFS peak at 1.58 Å in 5.3 *wt*% Co-N_4P SA sites locates between those of CoPc at 1.56 Å and CoP at 1.83 Å, confirming that the Co-N-P bond exists on nitrogen-doped carbon nanowires network (**Figure 2d**). Compared with the Co foil, CoPc and CoP, no Co-Co bond peak was observed in EXAFS spectra, verifying that no Co nanoparticles or clusters exist in 5.3 *wt*% Co-N_4P SA sites (**Figure 2d**). These results demonstrate that all Co atoms are atomically dispersed on nitrogen-doped carbon nanowires network.

The FT-EXAFS fittings in R and K spaces were also carried out to reveal the atomic structure of 5.3 *wt*% Co-N_4P SA sites (**Figure 2e, 2f & Table S3**). The fitting analysis result shows that the average coordination number of Co atom for the first coordination shell is 4.0 ± 0.2, and the average Co-N bond length is 1.58 Å in the 5.3 *wt*% Co-N_4P SA sites. Wavelet transform (WT) of Co K-edge EXAFS oscillations was used to further prove the atomic dispersion of the Co atoms in 5.3 *wt*% Co-N_4P SA sites. The intensity maximum values at 6.8 and 5.3 $Å^{-1}$ are ascribed to Co-P and Co-Co bonds in the WT contour plots of Co foil and CoP standard samples, respectively (**Figure 2g & 2h**). The WT contour plot of 5.3 *wt*% Co-N_4P SA sites shows only one intensity maximum value at 4.1 $Å^{-1}$, attributed to both Co-N and Co-N-P bonds (**Figure i**). These results confirm the existence of Co-N-P bond in 5.3 *wt*% Co-N_4P SA sites. In detail, the isolatedly dispersed Co atoms are asymmetrically coordinated by four N atoms with one asymmetric P atom on the nitrogen-doped carbon nanowires network (**the *inset* of Figure 2f**).

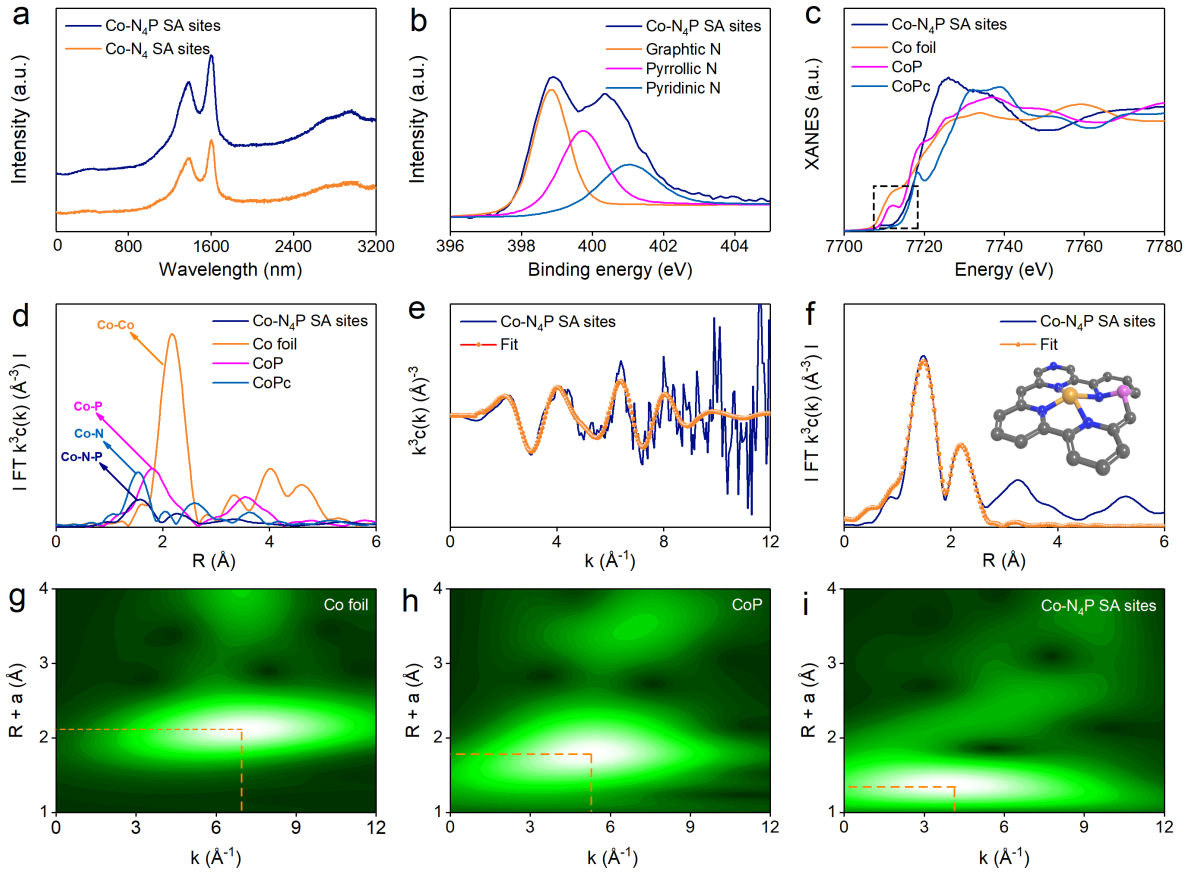

Figure 2. **Chemical structure and atomic coordination environment of 5.3 *wt*% Co-N4P SA sites.** (a) The Raman spectra of 5.5 *wt*% Co-N4 SA sites and 5.3 *wt*% Co-N4P SA sites. (b) High-resolution XPS spectrum of N 1s for 5.3 *wt*% Co-N4P SA sites. (c) Normalized XANES profiles, (d) EXAFS spectra in R space, (e) EXAFS fitting curve and (f) k^3-weight FT-EXAFS fitting curves for 5.3 *wt*% Co-N4P SA sites on nitrogen-doped carbon nanowires network at Co K-edge. (g-i) Wavelet transform of Co foil, CoP and 5.3 *wt*% Co-N4P SA sites on nitrogen-doped carbon nanowires network.

The catalytic performance of 5.3 *wt*% Co-N4P SA sites towards HCOOH dehydrogenation was investigated in a typical reaction set-up (**Figure S14**), and benchmarked with 2.8 *wt*% Co-N4 SA sites, 4.1 *wt*% Co-N4 SA sites and 5.5 *wt*% Co-N4 SA sites. Before evaluating HCOOH dehydrogenation performance, all the catalysts were pretreated under Ar/H2 (95/5 v/v) atmosphere at 280 °C for 30 min. The treated 2.8 *wt*% Co-N4 SA sites, 4.1 *wt*% Co-N4 SA sites, 5.5 *wt*% Co-N4 SA sites and 5.3 *wt*% SA Co-N4P sites show excellent dispersion in water (**Figure S15**). The HCOOH dehydrogenation begins as soon as catalyst (2.8 *wt*% Co-N4 SA sites, 4.1 *wt*% Co-N4 SA sites, 5.5 *wt*% Co-N4 SA sites or 5.3 *wt*% Co-N4P SA sites) and

HCOOH are mixed, even at the mild temperature condition (**Upper *inset* of Figure 3a**). Using 5.3 *wt*% Co-N_4P SA sites as a representative catalyst, we first optimized the reaction conditions of HCOOH dehydrogenation including catalyst concentration and HCOOH concentration (**Table S4 & S5**).

We find that all as-synthesized catalysts show high selectivity of over 99% towards HCOOH dehydrogenation. However, the 5.3 *wt*% Co-N_4P SA sites show the highest activity by following the order of 5.3 *wt*% Co-N_4P SA sites >> 5.5 *wt*% Co-N_4 SA sites > 4.1 *wt*% Co-N_4 SA sites > 2.8 *wt*% Co-N_4 SA sites (**Figure 3a**), and compared with other reported non-noble metal catalysts (**Table S6**), the 5.3 *wt*% Co-N_4P SA sites exhibit higher activity towards HCOOH dehydrogenation. Obviously, with increasing the Co loading amount of Co-N_4 SA sites, the HCOOH dehydrogenation reaction rate correspondingly increases. However, under the same amount of Co active sites, the catalytic activity of 5.3 *wt*% Co-N_4P SA sites is 5.0 times higher than that of 5.5 *wt*% Co-N_4 SA sites (**Figure 3a**). The gas chromatography (GC) result shows that produced gas from 5.5 *wt*% Co-N_4 SA sites and 5.3 *wt*% Co-N_4P SA sites are composed of H_2 and CO_2 with the mole ratio of 1/1, and no CO was detected in the gas mixture (CO detection limit: ~2 ppm) (**Figure 3b**).

Furthermore, HCOOH dehydrogenation reaction rate is closely related to reaction temperature, the HCOOH dehydrogenation reaction rate increases with the elevated temperature. The decomposition ratio of HCOOH nearly reaches 100%, and the TOF values of 5.3 *wt*% Co-N_4P SA sites are 2185.5, 986.8, 589.5 and 321.8 h^{-1} at 100 ºC, 90 ºC, 80 ºC and 70 ºC, respectively (**Figure 3c & 3d**). In addition, the slope value of the line plotted by the ln (rate) *versus* ln (C_{Co}) is 1.02 (**Figure S16**), where the rate and C_{Co} represent the HCOOH dehydrogenation rate and the 5.3 *wt*% Co-N_4P SA site concentration respectively, confirming that the HCOOH dehydrogenation is pseudo-first-order kinetic over 5.3 *wt*% Co-N_4P SA sites. These results verify that optimal low-cost Co-N_4P SA sites can be served as a promising candidate catalyst for thermocatalytic H_2 generation from liquid HCOOH.

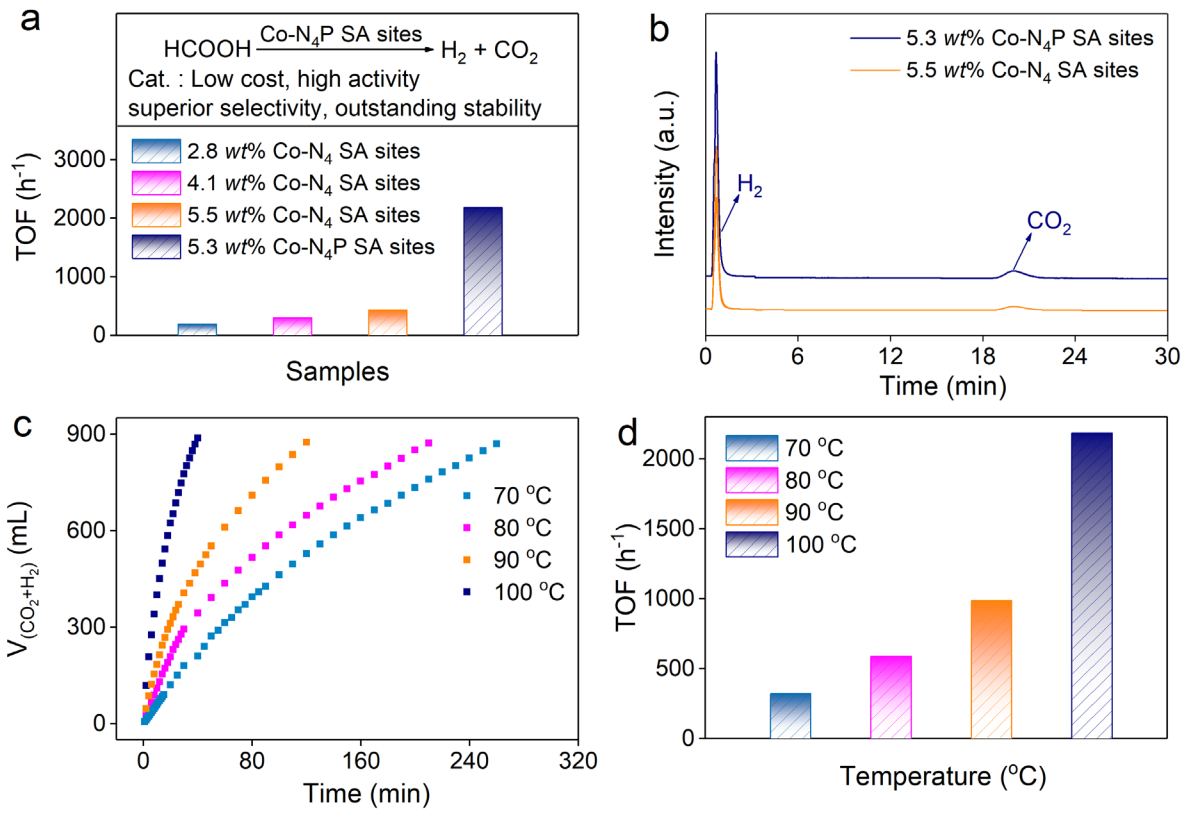

Figure 3. **HCOOH dehydrogenation performance of different catalysts**. (a) HCOOH decomposition catalyzed by 2.8 *wt*% Co-N4 SA sites, 4.1 *wt*% Co-N4 SA sites, 5.5 *wt*% Co-N4 SA sites and 5.3 *wt*% Co-N4P SA sites, respectively. (b) GC of generated mixture gas during the HCOOH dehydrogenation over 5.5 *wt*% Co-N4 SA sites and 5.3 *wt*% Co-N4P SA sites at 100 °C, respectively. (c) Effect of temperature on the catalytic activity of HCOOH dehydrogenation over 5.3 *wt*% Co-N4P SA sites from 70 to 100 °C. Reaction conditions: HCOOH, 0.8 mL; H_2O, 9.2 mL; Catalyst, 25 mg; *T*, as specified. (d) TOF of 5.3 *wt*% Co-N4P SA sites at different temperatures.

To investigate the HCOOH oxidation for H_2 generation on the 5.3 *wt*% Co-N4P SA sites, DFT calculations were performed. In 5.3 *wt*% Co-N4P SA sites, we notice that the bonding orbitals have been mostly focused on the Co SA sites (**Figure 4a**). The asymmetric introduction of the P atom has perturbed the electronic distributions near the Co sites, which dominates the anti-bonding orbitals. The Co sites and neighboring N atoms lead to the formation of a reactive region, which guarantees the electron transfer from the catalyst surface to the intermediates. The detailed electronic structure has been revealed by the projected partial density of states (PDOS) (**Figure 4b**). Notably, Co-3*d* orbitals exhibit a sharp peak

close to the Fermi level (E_F) at E_V -0.87 eV, which plays as the active site for the stable adsorptions of HCOOH. Meanwhile, the *s*, *p* orbitals of both N and C sites display the broad ban, which is able to achieve efficient site-to-site electron transfer. Notably, the broad P-3*s*, 3*p* orbitals show an evident overlapping with Co-3*d* orbitals and *s*, *p* orbitals of C, N atoms. The high electron density near E_F also leads to efficient electron transfer for the HCOOH oxidization.

For the Co SA sites, we have compared the electronic structure with different Co-based compounds (**Figure 4c**). It is noted that Co-3*d* orbitals in 5.3 *wt*% Co-N_4P SA sites have shown a much higher *d*-band center than those in Co metal and CoO, indicating the improved reactivity. The Co species in 5.3 *wt*% Co-N_4P SA sites has shown a similar electronic structure to that in Co_3O_4, indicating the high valence states of Co sites. Moreover, the PDOS of different types of N sites also confirms the electronic modulations induced by the introduction of asymmetric P sites and Co sites (**Figure 4d**). The graphitic N sites display the electron-rich feature with low reactivity. Notably, the *s*, *p* orbitals of the pyridinic N sites have demonstrated high electron density near the E_F. With the introduction of P atoms, N-*s*, *p* orbitals have downshifted. The anchoring of Co SA site has further induced the downshifting of N-*s*, *p* orbitals due to the electron transfer from Co to N sites. The pyrodinic N sites connecting Co SA sites and P atoms show the lowest position in PDOS.

For the key intermediates of HCOOH oxidization, the electron transfer efficiency determines the conversion of intermediates (**Figure 4e**). From the HCOOH towards CO_2*, the *s, p* orbitals of the intermediates demonstrate a nearly linear upshifting trend, supporting the smooth oxidation process on the 5.3 *wt*% Co-N_4P SA sites. Such a linear correlation also confirms that HCOO* is the key reactant during the HCOOH oxidation. To further unravel the reaction mechanism of HCOOH oxidation for H_2 generation, energetic investigations were performed. The adsorption energies of key intermediates HCOOH and proton have been compared in different sites on the 5.3 *wt*% Co-N_4P SA sites (**Figure 4f**). For the HCOOH, we notice that Co SA sites demonstrate the most stable adsorptions for HCOOH. Meanwhile, the nearby C and N sites both support a relatively strong binding trend with HCOOH, which is attributed to the formed electroactive region. As a comparison, the proton adsorption is mostly favored on P sites, both N and C sites have displayed an unfavored binding trend for proton, which hinders the dehydrogenation process. These different adsorption trends reveal that Co

SA sites act as the main active sites for HCOOH oxidation and the P sites are the key factor in promoting the dehydrogenation process. This combination guarantees highly efficient HCOOH oxidation and H_2 generation.

Figure 4. HCOOH hydrogenation over the 5.3 *wt*% Co-N_4P SA sites deciphered by DFT calculations. The 3D contour plot of electronic distribution near Fermi level of (a) 5.3 *wt*% Co-N_4P SA sites. Blue isosurface = bonding orbitals and green isosurface = anti-bonding orbitals. The PDOS comparison of 5.3 *wt*% Co-N_4P SA sites. Orange balls = Co, blue balls = N, pink balls = P and grey balls = C. (c) The comparison of Co-3*d* orbitals. (d) The site-dependent PDOS of N-*s, p*. (e) The PDOS of key intermediates for the oxidation of HCOOH. (f) The adsorption energies of HCOOH and H on different sites. (g) The reaction trend of HCOOH oxidation on Co-N_4P SA sites and Co-N_4 SA sites.

The reaction energies further confirm the high reaction preference for HCOOH oxidation

on the 5.3 *wt*% SA Co-N4P sites (**Figure 4g**). For both the Co-N4P and the Co-N4 SA sites, the initial dehydrogenation of HCOOH prefers the O-H dissociation than the C-H dissociation to form the HCOO*, where the formation of COOH* meets a large energy barrier of 0.43 eV and 1.53 eV, respectively. For the following C-H dissociation, Co-N4P SA sites show a subtle energy barrier of 0.08 eV, which is much smaller than that on Co-N4 SA sites (1.43 eV), leading to significantly improved catalytic performances for H_2 generation on Co-N4P SA sites. Although the Co-N4 shows a slightly lower reaction energy of -0.50 eV than that of -0.32 eV on Co-N4P, the larger energy barrier for the C-H dissociation significantly limits the catalytic performances of H_2 generation on Co-N4 SA sites. Therefore, the reaction energy comparison further supports the efficient HCOOH oxidation for H_2 generation on 5.3 *wt*% SA Co-N4P sites. The complete reaction pathway of HCOOH has been displayed in **Figure 5**.

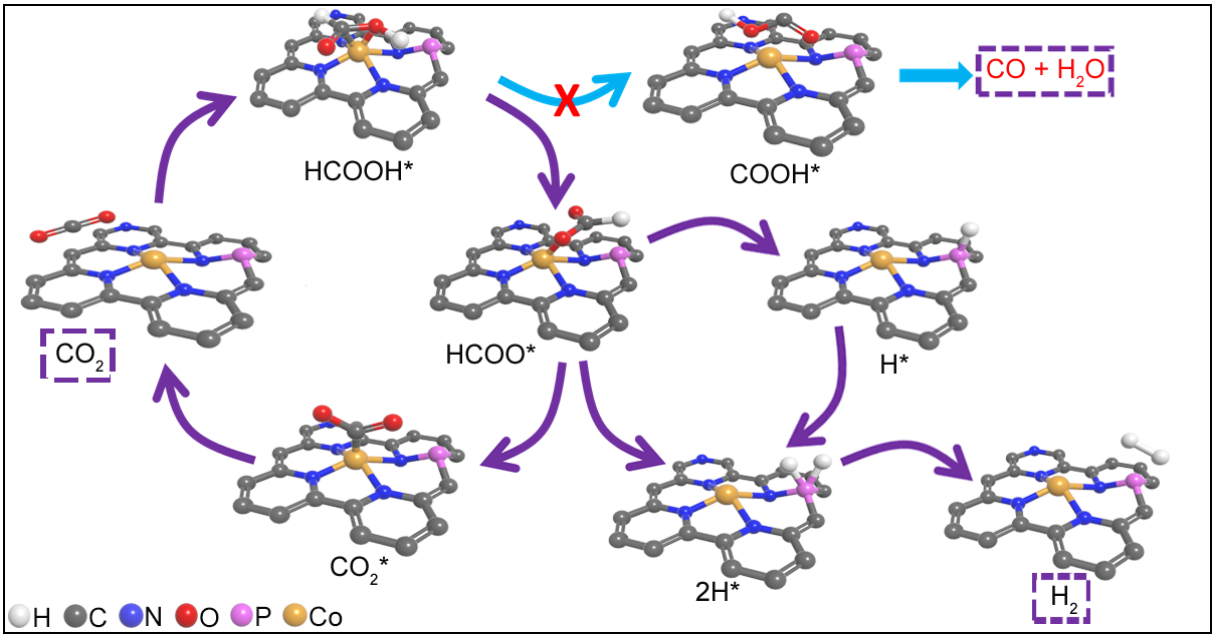

Figure 5. The selective dehydrogenation process of HCOOH on 5.3 *wt*% Co-N4P SA sites. White balls = H, grey balls = C, blue balls = N, red balls = O, pink balls = P and purple balls = Co.

The HCOOH dehydrogenation stability of 5.3 *wt*% Co-N4P SA sites was further evaluated in a 2.0 M aqueous HCOOH solution at 100 °C. The 5.3 *wt*% Co-N4P SA sites can maintain the initial selectivity, activity and excellent dispersion in aqueous HCOOH solution after five successive runs (**Figure S17**). The atomic phase of Co species and Co loading amounts of 5.3 *wt*% Co-N4P SA sites after five successive runs were analyzed by using STEM and ICP-AES,

respectively. There are no obvious changes in the size of Co species, and the size of Co species still remains atomic-level scale on the nitrogen-doped carbon nanowires network (**Figure S18**). After five successive runs, the HAADF-STEM image of 5.3 *wt*% Co-N_4P SA sites shows that there are still countless isolated bright spots representing Co atoms with the same Co amount (**Table S7**). These results indicate that the 5.3 *wt*% Co-N_4P SA sites are sufficiently stable and recycled for HCOOH dehydrogenation under mild condition.

Conclusions

In summary, we report a new strategy to synthesize a class of asymmetrically coordinated SA Co-N_4P sites for achieving highly efficient HCOOH dehydrogenation under the mild condition. We find that asymmetric coordination of SA Co sites is highly dependent on the pyrolysis way and feeding amounts of PPh_3 and $Co(NO_3)_2{\cdot}6H_2O$. The XAFS spectroscopy and XPS spectroscopy results confirm the Co atoms of SA Co-N_4P sites are coordinated by the four N atoms with one asymmetric P atom. The as-made SA Co-N_4P sites exhibit 100% selectivity, high activity (2185.5 h^{-1}), excellent hydrophilicity, and outstanding stability towards HCOOH dehydrogenation. The catalytic activity of SA Co-N_4 sites is increased from 429.0 h^{-1} to 2185.5 h^{-1} based on the asymmetrically coordinated way. DFT calculations unravel that the asymmetric P atoms enable the stable binding of proton simultaneously to accelerate the efficient dehydrogenation of HCOOH at the Co SA sites, revealing the optimal electronic structures for high activity and selectivity. This work supplies an advanced strategy to optimize the design of SA sites for broad applications in different catalytic reactions.

Supporting Information

Supporting Information is available from the Wiley Online Library or from the author.

Acknowledgements

This work was supported by the National Natural Science Foundation of China (Grant Nos. 11772257), the National Key R&D Program of China (2021YFA1501101), Shaanxi Science Foundation (Nos. 2021JM-356 and 2021JM-103), the National Science Fund for Distinguished Young Scholars (No. 52025133), Tencent Foundation through the XPLORER

PRIZE and the Research Fund of the State Key Laboratory of Solidification Processing (NPU), China (No. SKLSP202004), and the National Natural Science Foundation of China/RGC Joint Research Project (N_PolyU502/21).

Received: ((will be filled in by the editorial staff))
Revised: ((will be filled in by the editorial staff))
Published online: ((will be filled in by the editorial staff))

References

[1] T. M. Khanna, G. Baiocchi, M. Callaghan, F. Creutzig, H. Guias, N. R. Haddaway, L. Hirth, A. Javaid, N. Koch, S. Laukemper, A. Löschel, M. M. Z. Dominguez, J. C. Minx, *Nat. Energy* **2021**, *6*, 925.

[2] S. Chatterjee, K. W. Huang, *Nat. Commun.* **2020**, *11*, 1.

[3] H. Zhang, W. Cheng, D. Luan, X. W. Lou, *Angew. Chem. Int. Ed.* **2021**, *60*, 13177.

[4] J. Kosco, M. Bidwell, H. Cha, T. Martin, C. T. Howells, M. Sachs, D. H. Anjum, S. G. Lopez, L. Y. Zou, A. Wadsworth, W. M. Zhang, L. S. Zhang, J. Tellam, R. Sougrat, F. Laquai, D. M. DeLongchamp, J. R. Durrant, I. McCulloch, *Nat. Mater.* **2020**, *19*, 559.

[5] S. Liu, J. Liu, X. Liu, J. Shang, L. Xu, R. Yu, J. Shui, *Nat. Nanotechnol.* **2021**, *16*, 331.

[6] C. Ashworth, *Nat. Rev. Mater.* **2020**, *5*, 172.

[7] P. Zhou, H. Chen, Y. Chao, Q. Zhang, W. Zhang, F. Lv, L. Gu, Q. Zhao, N. Wang, J. Wang, S. Guo, *Nat. Commun.* **2021**, *12*, 4412.

[8] P. Preuster, C. Papp, P. Wasserscheid, *Acc. Chem. Res.* **2017**, *50*, 74.

[9] M. Li, Z. Zhao, Z. Xia, M. Luo, Q. Zhang, Y. Qin, L. Tao, K. Yin, Y. Chao, L. Gu, W. Yang, Y. Yu, G. Lu, S. Guo, *Angew. Chem. Int. Ed.* **2021**, *60*, 8243.

[10] D. Zhao, Y. Wang, C. L. Dong, Y. C. Huang, J. Chen, F. Xue, L. Guo, *Nat. Energy* **2021**, *6*, 388.

[11] A. H. Motagamwala, R. Almallahi, J. Wortman, V. O. Igenegbai, S. Linic, *Science* **2021**, *373*, 217.

[12] H. Fuse, H. Mitsunuma, M. Kanai, *J. Am. Chem. Soc.* **2020**, *142*, 4493.

[13] R. Li, Z. Liu, Q. T. Trinh, Z. Miao, S. Chen, K. Qian, W. Liu, *Adv. Mater.* **2021**, *33*, 2101536.

[14] T. Hou, Q. Luo, Q. Li, H. Zu, P. Cui, S. Chen,.Y. Lin, J. Chen, X. Zheng, W. Zhu, S. Liang, J. Yang, L.Wang, *Nat. Commun.* **2020**, *11*, 1.

[15] S. Kar, M. Rauch, G. Leitus, Y. Ben-David, D. Milstein, *Nat. Catal.* **2021**, *4*, 193.

[16] P. Zhou, Q. Zhang, Z. Xu, Q. Shang, L. Wang, Y. Chao, S. Guo, *Adv. Mater.* **2020**, *32*, 1904249.

[17] A. Weilhard, S. P. Argent, V. Sans, *Nat. Commun.* **2021**, *12*, 231.

[18] F. Valentini, V. Kozell, C. Petrucci, A. Marrocchi, Y. L. Gu, D. Gelman, L. Vaccaro, *Energy. Environ. Sci.* **2019**, *12*, 2646.

[19] G. Liu, P. Poths, X. Zhang, Z. Zhu, M. Marshall, M. Blankenhorn, K. H. Bowen, *J. Am. Chem. Soc.* **2020**, *142*, 7930.

[20] P. Zhu, H. Wang, *Nat. Catal.* **2021**, *4*, 943.

[21] F. Shen, R. L. Smith Jr, J. Li, H. Guo, X., Zhang, X. Qi, *Green Chem.* **2021**, *23*, 1536.

[22] X. Gu, Z. H. Lu, H. L. Jiang, T. Akita, Q. Xu, *J. Am. Chem. Soc.* **2011**, *133*, 11822.

[23] K. Tedsree, T. Li, S. Jones, C. W. A. Chan, K. M. K. Yu, P. A. J. Bagot, E. A. Marquis, G. D. W. Smith, S. C. E. Tsang, *Nat. Nanotechnol.* **2011**, *6*, 302.

[24] S. Zhang, O. Metin, D. Su, S. H. Sun, *Angew. Chem. Int. Ed*. **2013**, *52*, 3681.

[25] Z. L. Wang, J. M. Yan, Y. Ping, H. L. Wang, W. T. Zheng, Q. Jiang, *Angew. Chem. Int. Ed.* **2013**, *125*, 4502.

[26] H. Liu, Y. S. Yu, W. W. Yang, W. J. Lei, M. Y. Gao, S. J. Guo, *Nanoscale* **2017**, *9*, 9305.

[27] H. Liu, X. Y. Liu, W. W. Yang, M. Shen, S. Geng, C. Yu, Y. S. Yu, *J. Mater. Chem. A* **2019**, *7*, 2022.

[28] J. Wang, F. Xu, H. Jin, Y. Chen, Y. Wang, *Adv. Mater.* **2017**, *29*, 1605838.

[29] A. Mehmood, J. Pampel, G. Ali, H. Y. Ha, F. Ruiz-Zepeda, T. P. Fellinger, *Adv. Energy Mater.* **2018**, *8*, 1701771.

[30] H. Liu, X. Li, Z. Ma, M. Sun, M. Li, Z. Zhang, L. Zhang, Z. Tang, Y. Yao, B. Huang, S. Guo, *Nano Lett.* **2021**, *21*, 10284.

[31] C. Tang, A. E. Surkus, F. Chen, M. M. Pohl, G. Agostini, M. Schneider, M. Beller, *Angew. Chem. Int. Ed.* **2017**, *129*, 16843.

[32] M. F. Kuehnel, D. W. Wakerley, K. L. Orchard, E. Reisner, *Angew. Chem. Int. Ed.* **2015**, *54*, 9627.

[33] A. Boddien, D. Mellmann, F. Gärtner, R. Jackstell, H. Junge, P. J. Dyson, G. Laurenczy, R. Ludwig, M. Beller, *Science* **2011**, *333*, 1733.

[34] A. Boddien, B. Loges, F. Gartner, C. Torborg, K. Fumino, H. Junge, R. Ludwig, M. Beller, *J. Am. Chem. Soc.* **2010**, *132*, 8924.

[35] D. Mellmann, P. Sponholz, H. Junge, M. Beller, *Chem. Soc. Rev.* **2016**, *45*, 3954.

[36] K. Sordakis, C. Tang, L. K. Vogt, H. Junge, P. J. Dyson, M. Beller, G. Laurenczy, *Chem. Rev.* **2018**, *118*, 372.

[37] N. Onishi, M. Iguchi, X. Yang, R. Kanega, H. Kawanami, Q. Xu, Y. Himeda, Adv. *Energy Mater.* **2019**, *9*, 1801275.

[38] X. He, Q. He, Y. Deng, M. Peng, H. Chen, Y. Zhang, H. Ji, *Nat. Commun.* **2019**, *10*, 1.

[39] A. Wang, J. Li, T. Zhang, *Nat. Rev. Chem.* **2018**, *2*, 65.

[40] H. Liu, M. Shen, P. Zhou, Z. Guo, X. Liu, W. Yang, M. Gao, M. Chen, H. Guan, N. P. Padture, Y. Yu, S. Guo, S. Sun, *Nanoscale* **2021**, *13*, 9315.

[41] S. Ji, Y. Chen, X. Wang, Z. Zhang, D. Wang, Y. Li, *Chem. Rev.* **2020**, *120*, 11900.

[42] L. Han, L. Zhang, H. Wu, H. Zu, P. Cui, J. Guo, L. Wang, *Adv. Sci.* **2019**, *6*, 1900006.

[43] D. A. Bulushev, M. Zacharska, A. S. Lisitsyn, O. Y. Podyacheva, F. S. Hage, Q. M. Ramasse, L. G. Bulusheva, *ACS Catal.* **2016**, *6*, 3442.

[44] D. Janssen-Müller, C. Schlepphorst, F. Glorius, *Chem. Soc. Rev.* **2017**, *46*, 4845.

[45] A. Zitolo, V. Goellner, V. Armel, M. T. Sougrati, T. Mineva, L. Stievano, F. Jaouen, *Nat. Mater.* **2015**, *14*, 937.

[46] Y. Zhao, N. Yang, H. Yao, D. Liu, L. Song, J. Zhu, S. Li, L. Gu, K. Lin, D. Wang, *J. Am. Chem. Soc.* **2019**, *141*, 7240.

[47] Z. Y. Wu, S. L. Xu, Q. Q. Yan, Z. Q. Chen, Y. W. Ding, C. Li, S. H. Yu, *Sci. Adv.* **2018**, *4*, eaat0788.

[48] P. Chen, T. Zhou, L. Xing, K. Xu, Y. Tong, H. Xie, Y. Xie, *Angew. Chem. Int. Ed.* **2017**, *129*, 625.

[49] H. Yan, X. Zhao, N. Guo, Z. Lyu, Y. Du, S. Xi, R. Guo, C. Chen, Z. Chen, W. Liu, C. Yao, J. Li, S. Pennycook, W. Chen, C. Su, C. Zhang, J. Lu, *Nat. Commun.* **2018**, *9*, 3197.

[50] Y. Cao, S. Chen, Q. Luo, H. Yan, Y. Lin, W. Liu, L. Cao, J. Lu, J. Yang, T. Yao, S. Wei, *Angew. Chem. Int. Ed.* **2017**, *56*, 12191.

The coordination environments of atomically dispersed active sites are significant for modulating the activity and selectivity. A novel catalyst with asymmetrically coordinated Co-N_4P SA sites was first reported to achieve superior dehydrogenation catalysis of HCOOH with high activity, 100% selectivity, and outstanding stability under a mild condition. This work offers advanced insights into the design of efficient SA sites catalysts.

Hu Liu, Qian Lei, Ruoyan Miao, Mingzi Sun, Menggang Li, Zhenhui Ma, Liang Zhang, Gan Ye, Yong Yang, Yao Yao, Bolong Huang*, Shaojun Guo**

Asymmetric Coordination of Single-atom Co Sites Boosts Dehydrogenation Catalysis of HCOOH